nature structural & molecular biology

Organization of the archaeal MCM complex on DNA and implications for the helicase mechanism

Adam T McGeoch[1,2], Michael A Trakselis[1,2], Ronald A Laskey[1] & Stephen D Bell[1]

The homomultimeric archaeal mini-chromosome maintenance (MCM) complex serves as a simple model for the analogous heterohexameric eukaryotic complex. Here we investigate the organization and orientation of the MCM complex of the hyperthermophilic archaeon *Sulfolobus solfataricus* (Sso) on model DNA substrates. Sso MCM binds as a hexamer and slides on the end of a 3′-extended single-stranded DNA tail of a Y-shaped substrate; binding is oriented so that the motor domain of the protein faces duplex DNA. Two candidate β-hairpin motifs within the MCM monomer have partially redundant roles in DNA binding. Notably, however, conserved basic residues within these motifs have nonequivalent roles in the helicase activity of MCM. On the basis of these findings, we propose a model for the mechanism of the helicase activity of MCM and note parallels with SV40 T antigen.

In eukaryotes, the MCM complex has essential roles in both the initiation and elongation phases of DNA replication. The six distinct MCM subunits (MCM2–7) show sequence homology to one another and are therefore presumed to be derived from a common ancestor[1]. Archaea encode a DNA replication system that is in essence a stripped-down or ancestral version of the core eukaryotic machinery[2]. More specifically, archaea have simplified versions of the core initiator proteins Orc1 and Cdc6 on a single polypeptide, and most species encode a single MCM ortholog that forms a homomultimer. The majority of studies have been performed with the MCM of *Methanothermobacter thermoautotrophicus* (Mth)[3–5]. The Mth MCM is a homomultimer with a low level of ATPase activity that is substantially stimulated by DNA. The enzyme also has a 3′→5′ helicase activity that seems quite processive, as it can melt up to 500 base pairs of duplex DNA[3]. A subassembly of eukaryotic MCM subunits 4, 6 and 7 has processive helicase activity; however, the full heterohexameric MCM 2–7 does not[6–9].

Structural and hydrodynamic studies have shown that archaeal MCM proteins form ring-shaped complexes[3,10–12]. Analogy with other helicases, albeit of different families and activities, suggests that MCM encircles DNA to mediate DNA melting. Three-dimensional models and biochemical characterizations of multimeric helicases have suggested various mechanisms for unwinding DNA[13–15]. Structures of helicases related to the bacterial replicative helicase DnaB show that ATP hydrolysis may occur in an endless circular wave around the ring, with successive active sites occupied by ATP, occupied by ADP + P_i and empty[13]. Therefore, hydrolysis of ATP both influences the nucleotide occupancy status of neighboring binding sites and induces conformational alterations in the protein, facilitating its translocation along DNA. However, in contrast to MCM, DnaB has 5′→3′ helicase activity and belongs to a different family of helicases than MCM.

More recently, the structure of the SV40 large tumor antigen (Tag) has been solved in a variety of nucleotide-bound and free states[16,17]. Tag belongs to the superfamily 3 (SF3) class of helicases, and is therefore phylogenetically distinct from both DnaB and MCM[1]. Notably, Tag seems to use a distinctive mechanism for coupling ATP hydrolysis to movement. The structural work has indicated a concerted model for ATP hydrolysis, with all six subunits either simultaneously occupied by ATP or ADP or simultaneously empty, suggesting that the switching of all subunits among these states is coordinated. Notably, the switch in nucleotide partner seems to induce large-scale (up to 17-Å) movement of a positively charged β-hairpin motif in the AAA+ motor domain of Tag[17]. This has been proposed as the force that drives movement of Tag along DNA. Although no structural data are yet available about the motor domain of MCM, the crystal structure of the N-terminal domain has been solved[11]. This domain has β-hairpin motifs oriented into the central cavity of the protein that are similar to those found in the motor domain of Tag.

Here we investigate the relative orientations of MCM and DNA and the interactions between them. We show that the MCM monomer has a highly conserved candidate β-hairpin in the AAA+ motor domain of the protein. Furthermore, this motif, although dispensable for DNA binding by MCM, is essential for the helicase activity of the complex. Together with observations on the organization, orientation and loading of MCM on DNA, these data suggest mechanistic parallels between SV40 and MCM helicases.

[1]MRC Cancer Cell Unit, Hutchison MRC Research Centre, Hills Road, Cambridge, CB2 2XZ, UK. [2]These authors contributed equally toward this work. Correspondence should be addressed to S.D.B. (sb419@hutchison-mrc.cam.ac.uk).

Published online 14 August 2005; doi:10.1038/nsmb974

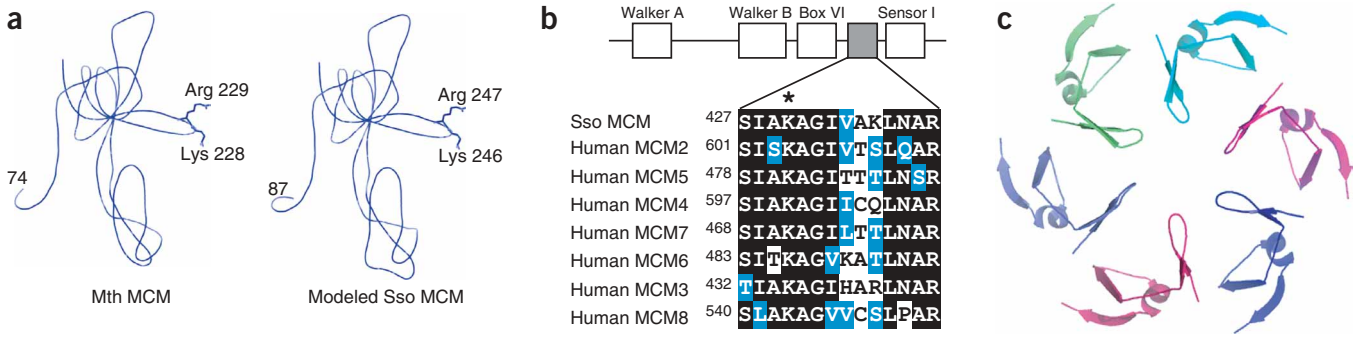

Figure 1 Two candidate β-hairpins in Sso MCM. (**a**) Left, the structure of domains B and C (residues 78–242) of the N-terminal region of Mth MCM. Right, the modeled structure of Sso MCM residues 87–260. Conserved basic residues at the tips of the β-hairpins are marked. (**b**) Sequence alignment of the candidate β-hairpins located between BoxVI and the sensor I motif in the AAA+ domain of MCMs. Black boxes, sequence identity; blue boxes, sequence homology; asterisk, the conserved lysine residue that was mutated to alanine for use in the experiments shown in **Figure 2**. (**c**) Structure of residues 505–547 of SV40 Tag showing the central β-hairpins located between BoxVI and the sensor I motif in the AAA+ fold. The image was created using PyMOL from PDB coordinates 1SVM.

RESULTS

Candidate β-hairpins and DNA binding

The structure of the N-terminal domain of Mth MCM contains a β-hairpin motif[11]. This motif is conserved in Sso MCM, allowing threading of residues 87–260 of Sso MCM onto the Mth MCM structure (**Fig. 1a**). This has facilitated the identification of conserved basic residues (Lys246 and Arg247) located at the tip of the hairpin. Mutation of these basic residues in the isolated N terminus of Mth MCM abrogate its ability to interact with DNA[11], but the effect of mutations in the context of the full-length molecule is not known.

Compared with canonical AAA+ proteins such as Cdc48, the sequences of the AAA+ modules of MCMs each have a short insertion between box VI and the ATP status–sensing sensor I motif (**Fig. 1b**). The sequence of this insertion is very highly conserved among archaeal and eukaryotic MCMs, and secondary structure predictions show that it probably primarily forms a β-strand. Notably, SV40 Tag helicase and other SF3 helicases also have a small insertion at the same location. Structural studies of SV40 Tag and papillomavirus E1 have revealed that this insertion forms a β-hairpin motif (**Fig. 1c**)[16–18]. To determine whether the candidate β-hairpins in MCM might have a role in DNA binding or helicase activity, we mutated conserved basic residues in both hairpins to alanine. Three altered proteins were produced: Sso MCM-N, MCM-C and MCM-NC, containing mutations in N-terminal (K246A R247A), C-terminal (K430A) or both N- and C-terminal (K246A R247A K430A) β-hairpin motifs, respectively. All three proteins were indistinguishable from wild-type protein with respect to heat stability, and gel filtration showed that all three mutants are found primarily as hexamer (**Fig. 2a**,**b** and data not shown).

The ATPase activity of the Mth MCM protein is stimulated by the presence of various DNA substrates[3–5]. Sso MCM has a relatively weak

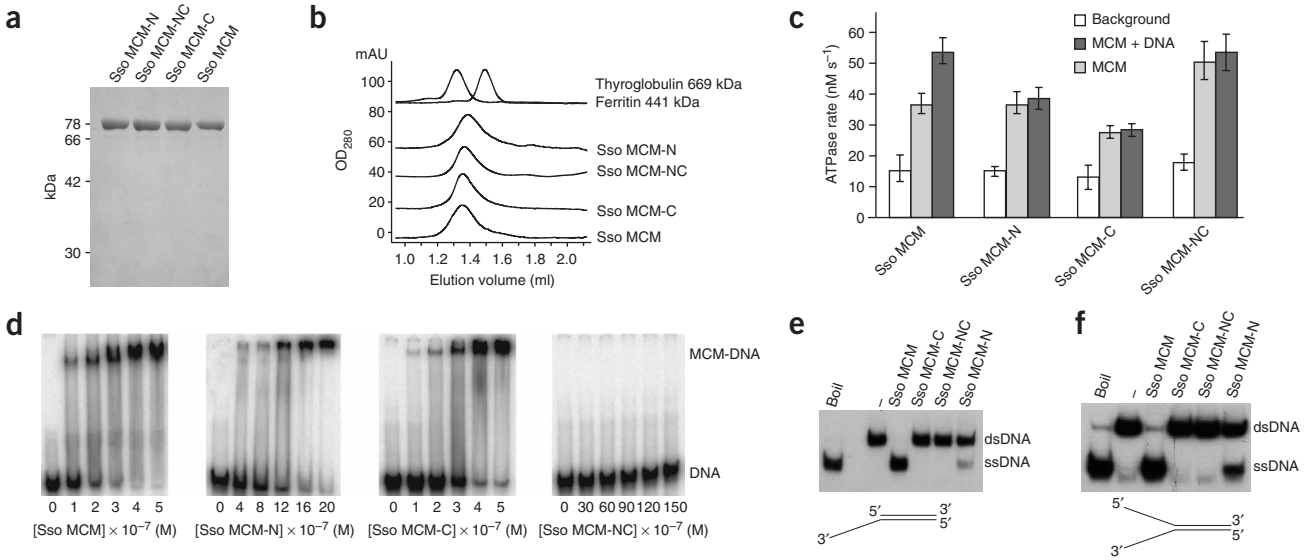

Figure 2 Biochemical characterization of Sso MCM. (**a**) SDS PAGE gel of 2 μg of wild-type or mutant MCM. (**b**) Gel filtration profile of wild-type and mutant MCM on a Superose 6 column (**c**) ATPase activity of the MCM mutants measured in the presence and absence of fork DNA. DNA moderately stimulated (1.5- to 1.8-fold) the ATPase activity of only wild-type MCM. (**d**) EMSA analysis of the binding of wild-type and mutant MCMs to a Y-shaped substrate; concentrations of protein monomers are indicated. (**e**) Results of helicase assays with 3 μM of wild-type or mutant MCM tested on 3′-tailed substrate. (**f**) Results of helicase assays with 3 μM of wild-type or mutant MCM tested on Y-shaped substrate.

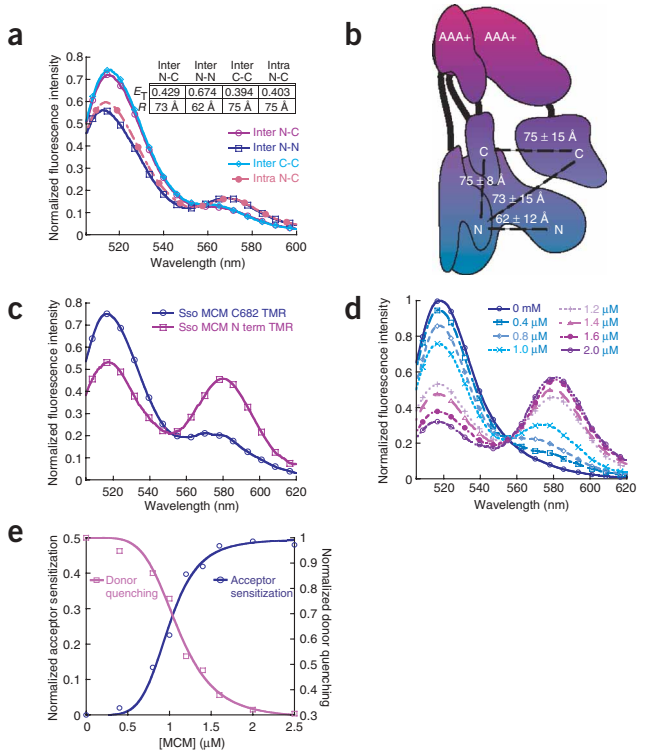

Figure 3 Architecture of MCM and orientation on DNA. (**a**) FRET data describing the internal orientation of the hexameric Sso MCM. Fluorescent labels were attached at the N terminus, Cys682 or both. Intermolecular and intramolecular experimental distances were then measured within the hexamer and corrected for statistical distributions; table depicts the resulting values. (**b**) Cartoon representation of two subunits of Sso MCM, based on the EM model of Mth MCM[12] and depicting the measured FRET distances. (**c**) Normalized fluorescent traces from TMR-labeled MCM, labeled at either the N terminus or Cys682, on a 3′ fluorescein–labeled DNA fork substrate. Qualitatively, the N terminus of Sso MCM is closer than the C terminus to the 3′ end of the DNA fork. (**d**) Fluorescence titration of the N-terminally TMR-labeled Sso MCM into 0.2 μM fluorescent DNA fork. (**e**) Acceptor sensitization and donor quenching maximums from **d** are fit to the Hill equation. For the acceptor sensitization and donor quenching traces, respectively, K_ms were 1.0 ± 0.1 μM and 1.1 ± 0.1 μM; fluorescence maximums were 0.50 ± 0.2 and 0.71 ± 0.03; and cooperativity constants were 5.5 ± 0.8 and 4.9 ± 0.9.

DNA-stimulated ATPase activity compared with MCMs from related species. ATPase activity of wild-type Sso MCM was 1.5- to 1.8-fold higher in the presence of DNA as measured by either an enzymatic coupled assay (**Fig. 2c**) or a radiometric assay (data not shown) at 50 °C. We propose that a conformational change in the MCM complex upon binding DNA allows for this increase in the rate of ATP hydrolysis, which is required for rapid unwinding. Notably, ATPase activities of the mutated proteins MCM-N, MCM-C and MCM-NC do not increase in the presence of DNA (**Fig. 2c**). This suggests important roles associated with DNA-stimulated ATP hydrolysis for the individual β-hairpins in both the N- and C-terminal domains.

We next used electrophoretic mobility shift assays (EMSAs) to test the ability of the hairpin mutant proteins to bind DNA. In contrast to data previously obtained with isolated Mth MCM N-terminal domain[11], we found that mutation of the N-terminal motif reduced rather than abrogated DNA binding by the full-length protein (wild-type K_d = 152 nM, MCM-N K_d = 1,208 nM; **Fig. 2d**). Similarly, mutation of the C-terminal candidate hairpin also reduced the affinity of MCM for DNA (MCM-C K_d = 343 nM; **Fig. 2d**). Therefore, in the context of the full-length protein neither motif is absolutely required for DNA binding; however, mutation of both motifs together abolished the ability of the mutant complex to bind DNA (**Fig. 2d**). The results shown in **Figure 2d** were obtained using a Y-shaped substrate; similar results were obtained with single-stranded (ss) and double-stranded (ds) DNA (data not shown). Thus, it seems that MCM has two regions of key importance in mediating protein–nucleic acid interactions. Mutation of either motif in isolation can be partially compensated for by the presence of the wild-type form of the other motif, but this redundancy is lost when both motifs are mutated.

Although neither motif was individually essential for DNA binding by Sso MCM, we wished to test the effects of the mutations on the helicase activity of the protein. We used two model substrates: one a partial duplex with a 3′-extended tail to permit helicase loading, the second a partial duplex with a Y shape arising from unpaired 3′ and 5′ tails. Similar results were obtained with both substrates (**Fig. 2e**,**f**). Sso MCM-NC, in which both candidate hairpins were mutated, had no detectable helicase activity even at high enzyme levels, consistent with its inability to bind DNA. The Sso MCM-N mutant retained detectable helicase activity, although this was reduced relative to the wild-type protein, again consistent with its reduced DNA-binding activity. In contrast, the Sso MCM-C mutant, although still able to bind DNA, is completely inactive as a helicase.

The ATPase rates, affinities for DNA and helicase activities of the β-hairpin mutants suggest distinct roles for the two hairpins. The low affinity of MCM-N for DNA, eight-fold lower than that of wild-type MCM, explains why this mutant showed no stimulation of ATPase activity in the presence of DNA and accounts for its reduced helicase activity. In contrast, the inability of MCM-C to unwind DNA could explain why this mutant shows no DNA-stimulated ATPase activity. Thus, the C-terminal candidate β-hairpin is not required for binding of Sso MCM to DNA but is essential for the ATP-catalyzed translocation of Sso MCM along DNA.

Solution architecture of MCM

Electron microscopy studies of archaeal MCM show that the protein forms a multimeric complex. But the precise stoichiometry of subunits has varied, with reports indicating that Mth MCM forms a hexamer[12], heptamer[10], double hexamer[3] or filament[19]. Modeling studies have suggested that subunits in a hexamer or heptamer are organized in parallel surrounding a central cavity. Mapping studies show that the N-terminal domains form a ring at one end of the hexamer and the AAA+ domains are located at the other end of the hexamer[12]. Finally, it has been proposed that the degenerate and poorly conserved C-terminal candidate helix-turn-helix motif folds back and is positioned at the midpoint of the hexamer[12]. Using this structural information as a guide, we wished to identify structural landmarks within Sso MCM and examine the topography of the complex on a DNA substrate.

We used fluorescence resonance energy transfer (FRET) to measure molecular distances at precise locations between and within the subunits of the Sso MCM complex. We specifically labeled the N terminus of Sso MCM by taking advantage of the large difference in pK_a between N-terminal amino groups and lysine residues; fluorescent labeling reactions with succinimidyl esters were performed at pH 6.8. Additionally, site-directed mutagenesis left a single accessible cysteine residue (Cys682) (Ellman's assay, see Methods, data not shown) available for labeling at the C terminus with maleimide

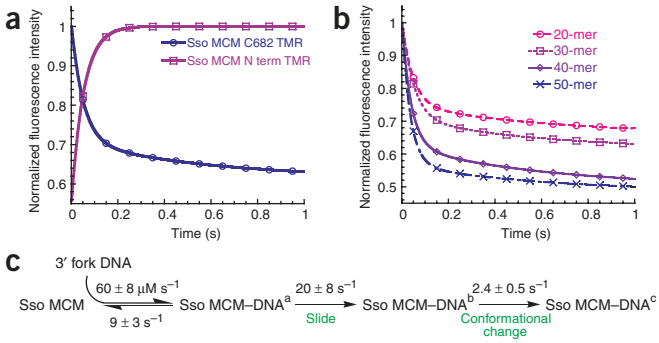

Figure 4 Loading of Sso MCM onto DNA. (**a**) Stopped-flow fluorescence traces of Sso MCM labeled with TMR at either the N terminus or Cys682 versus 3′ fluorescein–labeled fork DNA blocked with streptavidin as in orientation experiments (**Fig. 3**). (**b**) The effect of 3′ ssDNA length on normalized FRET values when loading MCM labeled with TMR at Cys682. (**c**) Simulation of the traces in **b** gives the corresponding rate constants. Initial binding of Sso MCM to DNA results in the complex termed Sso MCM–DNA[a]. This then slides toward duplex DNA, resulting in the complex termed Sso MCM–DNA[b]. The second exponential rate observed with the C-terminally labeled MCM may be associated with a conformational change in that domain of the protein after sliding, which would yield the complex termed Sso MCM-DNA[c].

derivatives of fluorescent dyes. Alexa 488 and Alexa 555 were used as the donor and acceptor and were specifically attached to the N terminus, Cys682 or both.

A mixed population of donor and acceptor Sso MCMs was then used for steady-state FRET experiments. Qualitatively, the distance from one N terminus to another was less than the distance from one C terminus to another or from an N to a C terminus in the hexameric form of MCM (**Fig. 3a**,**b**). Energy transfer values were measured and background values subtracted and corrected for the statistical distribution of the hexameric population. As an internal control for the statistical corrections, intramolecular FRET was measured on a doubly labeled subunit labeled at the N terminus with Alexa 488 and at Cys682 with Alexa 555, and this provided another distance measurement. Distances between the donor- and acceptor-labeled N and C termini were virtually identical to a reciprocally labeled population (data not shown). Absolute distances measured within the hexamer have errors of no more than 20% for intermolecular FRET and 10% for intramolecular FRET. The resulting distance values are in good agreement with the electron microscopy model of Mth MCM[12], providing substantial credibility to this analysis and corroboration for the arrangement of subunits within the hexamer.

Orientation of the MCM hexamer on DNA

Although MCM will bind and unwind many different types of DNA substrates, a free 3′ end of ssDNA substantially increases its activity. Biochemical analyses have shown a 3′→5′ polarity for DNA during unwinding[3–5,20]. We therefore wished to examine the orientation of Sso MCM on DNA and to determine whether Sso MCM moves along DNA with the N- or C-terminal end of the hexamer proximal to the dsDNA. To address these questions, we used a Y-shaped model DNA substrate with the free 3′ end derivatized with the donor fluorescein and a tetramethylrhodamine-labeled MCM at either the N or the C terminus. Measured steady-state FRET distances within the hexamer provided points of reference for the orientation experiment. The double-stranded region of the DNA fork had a biotin attached to the 5′ end, which in conjunction with streptavidin created a steric block that prevented loading of Sso MCM onto the double-stranded end. The streptavidin-blocked fluorescent forked DNA substrate was then incubated with Sso MCM hexamers derivatized with acceptor fluorophores (TMR) at either the N or the C termini, and qualitative steady-state FRET was measured.

The N-terminally derivatized MCM showed a stronger FRET signal with the 3′ end of DNA than did the C-terminally derivatized MCM (**Fig. 3c**,**d**). Furthermore, FRET experiments in which the free 5′ end was labeled with fluorescein showed a much-reduced fluorescence value that was difficult to measure (data not shown). The qualitative FRET measurement is consistent with MCM loading on the 3′ ssDNA oriented with the AAA+ motor domain closer to the dsDNA and primed for unwinding activity; the N-terminal domain of MCM is subsequently positioned nearer the 3′ end of the DNA substrate. Distance was not measured quantitatively because of the complexity of the calculations in a system with one donor molecule and up to six acceptors. The orientation experiments described were performed in the presence of ADP to support MCM loading but not translocation; analogous results were obtained in the absence of nucleotide and in the presence of the nonhydrolyzable ATP analog ATPγ-S (data not shown).

Previous work on the Mth MCM has suggested that it can adopt a diverse range of structures, with hexamer, double-hexamer, heptamer and filamentous forms observed. Accordingly, we wished to determine the stoichiometry of the Sso MCM on a DNA substrate. To this end, we titrated the derivatized MCM into the fluorescent donor DNA at concentrations above the K_d value (**Fig. 3e**). The acceptor sensitization and donor quenching in the titration experiments were fit to the Hill equation with a coefficient of 5.5 ± 0.8. This is consistent with about six MCM monomers binding one DNA fork, providing support for a single hexamer bound to each DNA substrate.

MCM loading onto DNA

To examine loading onto DNA, presteady-state FRET values were measured between Sso MCM labeled with TMR at either the N terminus or Cys682 and the 3′ end of DNA labeled with fluorescein. The fluorescence traces for each labeled Sso MCM were normalized and compared (**Fig. 4a**). Sso MCM labeled at the N terminus shows a single exponential increase in fluorescence (observed rate, 22.4 ± 0.2 s^{-1}), whereas Sso MCM labeled at Cys682 shows two exponential decreases in fluorescence (observed rates, 21.6 ± 0.2 s^{-1} and 2.4 ±

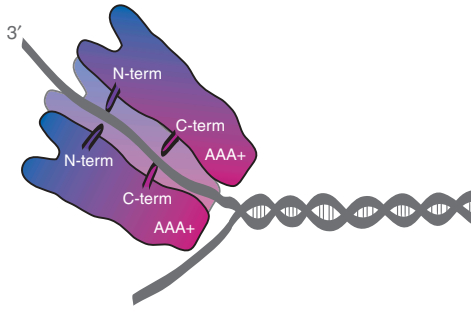

Figure 5 Cutaway model of MCM binding to DNA. The proposed β-hairpins in both the N- and C-terminal domains that are important for DNA binding, ATP hydrolysis and helicase activity are highlighted. The hexameric MCM is oriented such that the AAA+ motor domain is closer to the dsDNA and the N-terminal domain is closer to the 3′ ssDNA.

0.1 s^{-1}). Halving or doubling the Sso MCM concentration did not affect the observed rate constants, suggestive of a first-order kinetic step (data not shown). The fluorescence amplitudes of the differently labeled Sso MCMs were opposite in magnitude, suggesting that the N terminus was approaching the 3′ end of the DNA and the C terminus was moving farther away. This can be explained as the AAA+ domain binding the 3′ end of the DNA and the hexamer then sliding toward the duplex region. The similarity in the initial exponential rates between the two experiments corresponds to the sliding step (**Fig. 4c**). The second exponential rate observed with the C-terminally labeled MCM may be associated with a conformational change in that domain of the protein after sliding (**Fig. 4c**).

To verify these conclusions, the experiment using Sso MCM labeled with TMR at Cys682 was repeated with different lengths of 3′ fluorescein–labeled ssDNA (**Fig. 4b**). As the length of the ssDNA region increased, so did the associated change in fluorescence. This eliminates the possibility that Sso MCM binds specifically to fluorescein on the 3′ end, instead suggesting that it initially binds the 3′ end and slides along ssDNA in the absence of ATP until the AAA+ domain contacts duplex DNA. A kinetic mechanism for loading Sso MCM onto fork DNA was simulated using the K_d for binding to DNA and the observed presteady-state rates (**Fig. 4c**).

It should be noted that formation of a double hexamer may be possible with longer DNA substrates and that the composition of MCM *in vivo* is currently unknown. Nevertheless, the presteady-state and steady-state fluorescence data support a model in which the AAA+ domain of an Sso MCM hexamer initially binds the 3′ end of ssDNA and slides along until it reaches duplex DNA, where the C terminus undergoes an unknown conformational change. Notably, the orientation of Sso MCM on DNA is confirmed by presteady-state results showing the AAA+ motor domain oriented toward the duplex region of DNA and the N-terminal ring domain trailing behind it (**Fig. 5**).

DISCUSSION

Here we show that the Sso MCM has two principal DNA-binding sites, a β-hairpin in the N-terminal domain and a highly conserved region in the C-terminal motor domain, which we propose forms a β-hairpin. Mutation of absolutely conserved basic residues in either region resulted in a quantitative reduction in DNA binding by the full-length molecule. Crucially, however, mutation of both regions abrogates binding by MCM. Notably, the two mutations have different effects on the helicase activity of the MCM. The N-terminal mutation results in substantially reduced helicase activity, in agreement with the mutant protein's approximately eight-fold reduced affinity for DNA. In contrast, although the C-terminal mutation reduces affinity for DNA only about 2.5-fold, mutant proteins of this type have no detectable helicase activity. This suggests that the C-terminal candidate β-hairpin motif has a pivotal role in the transduction of ATP hydrolysis to translocation of MCM on DNA. In light of this, it may be possible to draw an analogy between MCM and the phylogenetically distinct superfamily 3 helicases exemplified by SV40 Tag. The SF3 helicases have a β-hairpin motif at precisely the same position in their primary sequence as the motif in MCM[16–18]. Furthermore, in SV40 Tag this β-hairpin changes position depending on whether ATP, ADP or no nucleotide is bound by the helicase, suggesting that this motif may be responsible for the 'power stroke' of the helicase. We speculate, therefore, that SF3 helicases and MCMs may share a common mode of action.

SV40 Tag forms a double hexamer at the SV40 origin of replication such that individual hexamers are positioned head to head, with N-terminal domains facing each other[16]. Structural studies of Mth MCM suggest that this molecule can also form a double hexamer with N-N joining of hexamers[11]. Our determination of the orientation of MCM on ssDNA strengthens the MCM-Tag analogy, showing that MCM, like Tag, moves along DNA in the 3′→5′ direction with the motor domain leading. There has been considerable debate about the nature of MCM's helicase activity, including proposals that the helicase acts on a single-stranded template or as double-strand pump. It should be stressed that all experiments testing the ability of MCM to translocate on dsDNA require a 3′-extended tail for loading of MCM onto the substrate[21,22]. Thus, the polarity of MCM that we have determined will be relevant to both single- and double-strand translocation models.

Finally, our studies of the homomultimeric archaeal MCM are likely to be informative regarding the mechanistic basis of action of the more complex eukaryotic heterohexameric MCMs, MCM2–7. The proposed C-terminal β-hairpin is very highly conserved among both homomultimeric and heteromultimeric MCMs (**Fig. 1b**). Furthermore, MCM8 has recently been discovered in higher eukaryotes[23], and like the archaeal MCMs, MCM8 is a homomultimer, has helicase activity and has a high basal ATPase activity that is only modestly stimulated by DNA. Moreover, MCM8 also has the characteristic insertion between BoxVI and sensor I (ref. 24), suggesting that β-hairpin structures are mechanistically essential in a variety of homologous helicases.

METHODS

Materials and their sources. Oligonucleotide primers and substrates were purchased from Sigma Genosys; sequences are available on request. A Y-shaped DNA substrate blocked with streptavidin at the 5′ end of the duplex region and labeled with fluorescein at the 3′ end was used as the DNA substrate in the fluorescent orientation experiments. Tetramethylrhodamine-5-malemide, 5-carboxytetramethylrhodamine succinimidyl ester (TMR), Alexa 488 succinimidyl ester, Alexa 488 maleimide, Alexa 555 succinimidyl ester and Alexa 555 maleimide were obtained from Molecular Probes. ADP, ATP, streptavidin, phosphoenolpyruvate, NADH and pyruvate kinase and lactate dehydrogenase enzymes were from Sigma. All other chemicals were of analytical grade or better. Labeling buffer consisted of 25 mM HEPES, 150 mM NaCl and 10 mM $MgCl_2$ at either pH 6.8 or pH 7.5. Storage buffer consisted of labeling buffer with 10 mM BME at pH 7.5.

Cloning, protein purification and protein labeling. The full-length Sso MCM open reading frame was amplified by PCR, adding AseI and XhoI restriction sites at the 5′ and 3′ ends of the open reading frame, respectively. The PCR product was digested with AseI and XhoI and ligated into pET30a digested with NdeI and XhoI. Mutants of Sso MCM were generated using the Quick Change protocol (Stratagene). The identities of the plasmid constructs were confirmed by DNA sequencing (MRC Geneservice).

BL21DE3 Rosetta *E. coli* transformed with the various MCM plasmids were grown at 37 °C to an OD_{600} of 0.6, induced with 0.6 mM IPTG and grown for an additional 6 h. Cells were spun down and resuspended in 1× TBS with 3 mg ml^{-1} lysozyme. After sonication, the supernatant was incubated at 70 °C for 30 min. The supernatant was then passed over a Mono Q column using an AKTA Prime system (Amersham Bioscience) and eluted at 0.3 M NaCl, followed by a heparin column eluted at 0.8 M NaCl. Finally, hexameric MCM was separated by gel filtration using a Superdex 200.

An Ellman assay[25] found that only two of the five cysteines of Sso MCM are accessible for modification. Mutation of C642A in Sso MCM resulted in only one cysteine (Cys682) being accessible (data not shown). Previous experiments have shown that the three cysteine residues toward the N terminus are involved in a zinc finger motif responsible for DNA binding and resistant to modification[26]. Sso MCM–C642A was labeled at the free cysteine residue (Cys682) with TMR or with Alexa 488 or Alexa 555 maleimides in labeling buffer at pH 7.5. Cysteine-labeled proteins were then quenched with 10 mM BME, put through a spin column and extensively dialyzed in storage buffer to remove excess label. To label the N terminus of Sso MCM, proteins were

labeled with TMR or with Alexa 488 or Alexa 555 succinimidyl esters in labeling buffer at pH 6.8 for 1 h. The lower pK_a of the N-terminal amino group (6.8) compared to those of the epsilon amino groups of lysines (8.0) resulted in the specific labeling of the N terminus at pH 6.8. Doubly labeled MCM was first labeled at the N terminus and then at Cys682, as described above. The degree of labeling was determined by UV spectrophotometry and found to be close to 1 for all labeled forms of Sso MCM. The fluorescent labels at both the N terminus and Cys682 were identified by ESI-MS of the tryptic digestion (MRC LMB Mass Spectrometry Facility). The ability of all mutants in both the unlabeled and fluorescence-labeled forms to unwind duplex DNA was verified in an unwinding assay (data not shown).

Structural modeling and alignment. The homology-based model of the N-terminal domain of Sso MCM was generated using SWISS MODEL[27]. The figure was prepared using PyMOL (http://pymol.sourceforge.net). The sequence alignment was generated with Pileup (GCG software package) and shaded using the BOXSHADE server (http://www.ch.embnet.org/software/BOX_form.html).

ATPase assay. Steady-state enzymatic coupled ATPase assays were performed essentially as described previously[28]. Specifically, Sso MCM (1 μM) was added to a cocktail containing 1.5 mM ATP, 3.3 mM phosphoenolpyruvate, 200 μM NADH and approximately 1 unit each of pyruvate kinase and lactate dehydrogenase in reaction buffer. After determination of the basal hydrolysis rate, fork DNA was added (500 nM final concentration) and the rate of ATP hydrolysis obtained. The ATPase hydrolysis rates of Sso MCM were verified by radiometric assay using [γ-^{32}P]ATP as described previously[29].

Probe for electrophoretic mobility shift assays and helicase assays. Top-strand oligonucleotides (100 ng) were radiolabeled with 30 μCi of [γ-^{32}P]ATP (6,000 Ci mmol^{-1}) using T4 polynucleotide kinase. After annealing to the complementary strand, the probe was gel purified. Probes both had 44 bases of dsDNA with either a single 3′ 44-base tail or both 3′ and 5′ 44-base tails forming a fork.

Electrophoretic mobility shift assay. EMSAs were performed in a 20 μl reaction volume containing 30 mM Tris acetate (pH 8), 75 mM NaCl, 50 mM potassium acetate, 10 mM magnesium acetate, 1 mM dithiothreitol, 5% glycerol, 0.5 nM DNA probe. Binding reactions were immediately loaded on a 5% polyacrylamide gel in 1× TBE. Gels were run for 90 min at 13 V cm^{-1} before drying and phosphorimagery.

Helicase assay. Reactions were performed in a 10 μl reaction volume containing 30 mM Tris acetate (pH 8), 75 mM NaCl, 50 mM potassium acetate, 10 mM magnesium acetate, 1 mM dithiothreitol, 0.5 nM DNA probe and 3 μM of the indicated protein. Reactions were incubated at 65 °C for 30 min before addition of 10 μl stop buffer (100 mM EDTA, 0.5% SDS, 0.1% bromophenol blue and 50% glycerol). Aliquots were then loaded on a 10% polyacrylamide gel in 1× TBE 0.1% SDS. Gels were run for 45 min at 15 V cm^{-1} before drying and autoradiography.

Gel filtration analysis. Protein (50 μl at a concentration of 6 μM) was applied to a Superose 6 gel filtration column (PC3.2/30; Amersham Biosciences, Inc.) equilibrated with 20 mM Tris (pH 8), 150 mM sodium chloride and 1 mM dithiothreitol, and absorbance at 280 nm was monitored.

Steady-state fluorescence spectroscopy. Steady-state fluorescence experiments were performed on a Perkin Elmer spectrofluorimeter thermostated to 25 °C. The excitation wavelength was 485 nm and the emission was monitored from 505–630 nm during an average of four scans. The slits were adjusted accordingly between 2.5 and 5 nm to keep the spectrum within range.

MCM subunit arrangement. A 1:1 mixture of donor- and acceptor-labeled MCM labeled at either the N terminus or Cys682 was allowed to equilibrate in solution (total concentration 1.2 μM). The background fluorescence caused by direct excitation of the acceptor at 485 nm was subtracted from all fluorescence traces. Statistical analyses determined that 64 different confirmations of a donor- and acceptor-labeled hexamer existed in solution. Within that population, there were zero to three individual FRET events within individual hexamers. Individual FRET events are defined as energy transfer to a single acceptor or to the average of two acceptors. This leads to reduction of the theoretical energy transfer (E_T) value by a factor of 0.65 according to the equation:

$$E_{T(observed)} = 0.65 \times E_{T(theoretical)}$$

Intramolecular FRET on the doubly labeled MCM was measured in a dilute solution with an eight-fold excess of unlabeled protein to minimize any intermolecular FRET background within the hexamer. Fluorescence resonance energy transfer (FRET) was calculated according to the following equations (ref. 30):

$$R = R_0 \sqrt[6]{\frac{1}{E_T} - 1}$$

$$E_T = \left(1 - \frac{F_{DA}}{F_D}\right)$$

where E_T is the transfer efficiency of the FRET process and F_{DA} and F_D are the fluorescent intensities of the Alexa 488 donor in the presence and absence, respectively, of the Alexa 555 acceptor. R is the Förster distance between the donor and acceptor and R_0 is the Förster distance at which the transfer efficiency is 50%, which is calculated to be 70 Å for this system using the equation:

$$R_0 = 2.11(\phi_D \kappa^2 \eta^{-4} J)^{1/6}$$

where ϕ_D is the quantum yield of the donor, κ^2 is the orientation factor, η is the refractive index of the medium and J is the overlap integral between the fluorescence spectrum of the donor and the absorption spectrum of the acceptor. κ^2 relates the relative orientations of the donor and acceptor pair and has a value between 0 and 4. For a freely rotating probe, κ^2 is assumed to be 2/3 (ref. 30). The rotational freedom of the probe is measured using steady-state fluorescence polarization spectroscopy. All the various labeled MCM proteins have anisotropy values less than 0.3, consistent with a freely rotating probe[31].

MCM orientation on DNA. Titrations were performed by sequential addition of a high concentration of Sso MCM to a fixed concentration of fluorescein-labeled DNA fork (0.2–1.0 μM) and were allowed to equilibrate before measuring the spectrum for a minimum of 5 min. The background fluorescence caused by direct excitation of the TMR acceptor at 485 nm was measured in a separate titration and subtracted using the supplied software (Perkin Elmer). The relative distances between the fluorescein on the 3′ end of the DNA fork and the donor TMR on either the N terminus or Cys682 of MCM were determined by FRET only qualitatively using both donor quenching and acceptor sensitization. Stoichiometry of the MCM complex on DNA was determined using KaleidaGraph (Synergy Software) to fit the acceptor sensitization maximums to the Hill equation:

$$v = \frac{F_{max} \times S^H}{K_{0.5}^H \times S^H}$$

where F_{max} is the fluorescence maximum, S is the MCM concentration, $K_{0.5}$ is one-half the fluorescence maximum and H is the Hill coefficient.

Presteady-state fluorescence spectroscopy. Stopped-flow fluorescence experiments were performed on an Applied Photophysics (Leatherhead) SX.18MV stopped-flow reaction analyzer in fluorescence mode at the constant temperature of 25 °C. The samples were excited at 480 nm, and a 530 nm cutoff filter was used to collect 1,000 oversampled data points detecting only TMR fluorescence. The excitation path length was 3 mm. The observed traces were fit to one or two exponentials using the supplied software. Kinetic simulations were performed using KinTekSim (Kintek Corp.). The simulated rate constants were optimized and then individually varied to determine the relative importance of the values to the quality of the simulation.

Accession codes. BIND identifiers (http://bind.ca): 315461, 315463.

ACKNOWLEDGMENTS

Work in the laboratory of S.D.B. is supported by the Medical Research Council. A.T.M. was additionally funded by Cambridge Clinical School. M.A.T. would

also like to thank the Royal Society for generous funding. We thank N. Thorne for help with statistical distribution corrections and Z. Kelman for stimulating discussions.

COMPETING INTERESTS STATEMENT

The authors declare that they have no competing financial interests.

Received 18 May; accepted 14 July 2005
Published online at http://www.nature.com/nsmb/

1. Iyer, L.M., Leipe, D.D., Koonin, E.V. & Aravind, L. Evolutionary history and higher order classification of AAA plus ATPases. *J. Struct. Biol.* **146**, 11–31 (2004).
2. Kelman, L.M. & Kelman, Z. Archaea: an archetype for replication initiation studies? *Mol. Microbiol.* **48**, 605–616 (2003).
3. Chong, J.P.J., Hayashi, M.K., Simon, M.N., Xu, R.M. & Stillman, B. A double-hexamer archaeal minichromosome maintenance protein is an ATP-dependent DNA helicase. *Proc. Natl. Acad. Sci. USA* **97**, 1530–1535 (2000).
4. Kelman, Z., Lee, J.K. & Hurwitz, J. The single minichromosome maintenance protein of *Methanobacterium thermoautotrophicum* Delta H contains DNA helicase activity. *Proc. Natl. Acad. Sci. USA* **96**, 14783–14788 (1999).
5. Shechter, D.F., Ying, C.Y. & Gautier, J. The intrinsic DNA helicase activity of *Methanobacterium thermoautotrophicum* Delta H minichromosome maintenance protein. *J. Biol. Chem.* **275**, 15049–15059 (2000).
6. Ishimi, Y.A. DNA helicase activity is associated with an MCM4, -6, and -7 protein complex. *J. Biol. Chem.* **272**, 24508–24513 (1997).
7. You, Z.Y., Komamura, Y. & Ishimi, Y. Biochemical analysis of the intrinsic Mcm4-Mcm6-Mcm7 DNA helicase activity. *Mol. Cell. Biol.* **19**, 8003–8015 (1999).
8. Lee, J.K. & Hurwitz, J. Isolation and characterization of various complexes of the minichromosome maintenance proteins of *Schizosaccharomyces pombe*. *J. Biol. Chem.* **275**, 18871–18878 (2000).
9. Lee, J.K. & Hurwitz, J. Processive DNA helicase activity of the minichromosome maintenance proteins 4, 6, and 7 complex requires forked DMA structures. *Proc. Natl. Acad. Sci. USA* **98**, 54–59 (2001).
10. Yu, X. *et al.* The *Methanobacterium thermoautotrophicum* MCM protein can form heptameric rings. *EMBO Rep.* **3**, 792–797 (2002).
11. Fletcher, R.J. *et al.* The structure and function of MCM from archaeal *M. thermoautotrophicum*. *Nat. Struct. Biol.* **10**, 160–167 (2003).
12. Pape, T. *et al.* Hexameric ring structure of the full-length archaeal MCM protein complex. *EMBO Rep.* **4**, 1079–1083 (2003).
13. Soultanas, P. & Wigley, D.B. Unwinding the 'Gordian knot' of helicase action. *Trends Biochem. Sci.* **26**, 47–54 (2001).
14. Laskey, R.A. & Madine, M.A. A rotary pumping model for helicase function of MCM proteins at a distance from replication forks. *EMBO Rep.* **4**, 26–30 (2003).
15. Kaplan, D.L. & O'Donnell, M. Twin DNA pumps of a hexameric helicase provide power to simultaneously melt two duplexes. *Mol. Cell* **15**, 453–465 (2004).
16. Li, D.W. *et al.* Structure of the replicative helicase of the oncoprotein SV40 large tumour antigen. *Nature* **423**, 512–518 (2003).
17. Gai, D.H., Zhao, R., Li, D.W., Finkielstein, C.V. & Chen, X.S. Mechanisms of conformational change for a replicative hexameric helicase of SV40 large tumor antigen. *Cell* **119**, 47–60 (2004).
18. Abbate, E.A., Berger, J.M. & Botchan, M.R. The X-ray structure of the papillomavirus helicase in complex with its molecular matchmaker E2. *Genes Dev.* **18**, 1981–1996 (2004).
19. Chen, Y.J. *et al.* Structural polymorphism of *Methanothermobacter thermautotrophicus* MCM. *J. Mol. Biol.* **346**, 389–394 (2005).
20. Grainge, I., Scaife, S. & Wigley, D. Biochemical analysis of components of the pre-replication complex of *Archaeoglobus fulgidus*. *Nucleic Acids Res.* **31**, 4888–4898 (2003).
21. Shin, J.H., Jiang, Y., Grabowski, B., Hurwitz, J. & Kelman, Z. Substrate requirements for duplex DNA translocation by the eukaryal and archaeal minichromosome maintenance helicases. *J. Biol. Chem.* **278**, 49053–49062 (2003).
22. Kaplan, D.L., Davey, M.J. & O'Donnell, M. Mcm4,6,7 uses a "pump in ring" mechanism to unwind DNA by steric exclusion and actively translocate along a duplex. *J. Biol. Chem.* **278**, 49171–49182 (2003).
23. Johnson, E.M., Kinoshita, Y. & Daniel, D.C. A new member of the MCM protein family encoded by the human MCM8 gene, located contrapodal to GCD10 at chromosome band 20p12.3–13. *Nucleic Acids Res.* **31**, 2915–2925 (2003).
24. Maiorano, D., Cuvier, O., Danis, E. & Mechali, M. MCM8 is an MCM2–7-related protein that functions as a DNA helicase during replication elongation and not initiation. *Cell* **120**, 315–328 (2005).
25. Ellman, G.L. Tissue sulfhydryl groups. *Arch. Biochem. Biophys.* **82**, 70–77 (1959).
26. Poplawski, A., Grabowski, B., Long, S.F. & Kelman, Z. The zinc finger domain of the archaeal minichromosome maintenance protein is required for helicase activity. *J. Biol. Chem.* **276**, 49371–49377 (2001).
27. Schwede, T., Kopp, J., Guex, N. & Peitsch, M.C. SWISS-MODEL: an automated protein homology-modeling server. *Nucleic Acids Res.* **31**, 3381–3385 (2003).
28. Kaboord, B.F. & Benkovic, S.J. Dual role of the 44/62 protein as a matchmaker protein and DNA polymerase chaperone during assembly of the bacteriophage T4 holoenzyme complex. *Biochemistry* **35**, 1084–1092 (1996).
29. Trakselis, M.A., Berdis, A.J. & Benkovic, S.J. Examination of the role of the clamp-loader and ATP hydrolysis in the formation of the bacteriophage T4 polymerase holoenzyme. *J. Mol. Biol.* **326**, 435–451 (2003).
30. Selvin, P.R. Fluorescence resonance energy-transfer. *Methods Enzymol.* **246**, 300–334 (1995).
31. Hass, E., Katchalski-Katzir, E. & Steinberg, I.Z. Effect of the orientation of donor and acceptor on the probability of energy transfer involving electronic transitions of mixed polarization. *Biochemistry* **17**, 5064–5070 (1978).